

Determination of Mid-Infrared Refractive Indices of Superconducting Thin Films Using Fourier Transform Infrared Spectroscopy

Dip Joti Paul,^{*} Tony X. Zhou,[†] and Karl K. Berggren

Research Laboratory of Electronics, Massachusetts Institute of Technology, Cambridge, MA 02139, USA

In this work, we present a technique to determine the mid-infrared refractive indices of thin superconducting films using Fourier transform infrared spectroscopy (FTIR). In particular, we performed FTIR transmission and reflection measurements on 10-nm-thick NbN and 15-nm-thick MoSi films in the wavelength range of 2.5 to 25 μm , corresponding to frequencies of 12–120 THz or photon energies of 50–500 meV. To extract the mid-infrared refractive indices of the thin films from FTIR measurements, we used the Drude-Lorentz oscillator model to represent the dielectric functions of the films and implemented an optimization algorithm to fit these oscillator parameters, minimizing the error between the measured FTIR spectra and the simulated spectra calculated using the dielectric functions of the films. To evaluate the consistency of the extracted dielectric functions, we compared the refractive index values extrapolated from these dielectric functions in the UV to near-infrared wavelengths with the values separately measured using spectroscopic ellipsometry. For further validation, we calculated the sheet resistance of the films from their extracted Drude oscillator parameters and compared with the experimental values. This FTIR-based refractive index measurement approach can be extended to measure the refractive indices of thin films at wavelengths beyond 25 μm , which will be useful for designing highly efficient photon detectors and photonic devices with enhanced optical absorption in the mid- and far-infrared wavelengths.

Introduction

Mid-infrared spectroscopy has been instrumental in numerous scientific discoveries and commercial applications due to its unique ability to identify chemical bonds. The photon wavelength, ranging from 2.5 μm to 25 μm , is known as the mid-infrared spectrum [1, 2]. Molecules exhibit distinct absorption and emission patterns within this wavelength range due to the excitation of vibrational and rotational modes in their constituent chemical bonds. Hence, this wavelength spectrum is often referred to as the molecular fingerprint region. Consequently, the development of highly efficient mid-infrared photon detectors has received constant attention in recent years [3–6].

Compared to conventional semiconducting mid-infrared detectors, superconducting nanowire single-photon detectors (SNSPDs) offer significant advantages in photon-starved environments due to their unique ability to resolve single-photon quanta and maintain extremely low dark count rates [7]. Therefore, efficient mid-infrared SNSPDs will be valuable in a broad range of applications related to astronomy [8], dark matter search [7, 9], LIDAR [10], biological [11], and environmental sensing [10]. However, the detection efficiency of SNSPDs depends on their photon absorption efficiency and internal detection efficiency. As the wavelength extends into the mid-infrared spectrum, the photon absorption efficiency of SNSPDs drops below 5%, primarily due to the monotonic decrease in the absorption coefficient of the superconducting material with increasing wavelength [3, 12, 13]. However, the free-space coupling

and absorption of mid-infrared photons with planar μm^2 -area SNSPD geometries can be improved by incorporating optical cavities [5], impedance-matched antennas [14], and metamaterials [15]. Designing such optical elements, however, requires knowledge of the mid-infrared refractive indices of the SNSPD material.

In this work, we characterized the mid-infrared optical properties of 10-nm-thick NbN and 15-nm-thick MoSi films. NbN is a polycrystalline superconducting material and it has been widely used in SNSPDs and superconducting circuits [12, 16]. While there have been previous demonstrations of mid-infrared SNSPDs using NbN [17, 18], the photon absorption efficiency was not optimized in those works. In addition, amorphous superconducting materials, such as MoSi and WSi, are considered ideal for sensing low-energy infrared photons [3, 4, 19]. SNSPDs based on MoSi have been demonstrated to detect 5 μm wavelength photons [19], and more recently, WSi thin films have been used to detect photons with a wavelength of 29 μm [4]. These studies also lack optimization of photon absorption efficiency in SNSPDs, as there have been no reports to date on the mid-infrared optical properties of MoSi and WSi. Therefore, having knowledge of the mid-infrared refractive indices of these superconducting thin films will enable researchers to perform simulations and fabricate optical elements to improve photon absorption efficiency of SNSPDs in the mid-infrared spectrum.

The conventional approach to determining the complex refractive indices of thin-film materials is to use spectroscopic ellipsometry tools. However, commercially available ellipsometry tools typically operate in the wavelength range of visible to near-infrared. The complex refractive indices of NbN and MoSi in the wavelength range from visible to 5 μm have been reported previously using ellipsometry [12, 13, 20]. However, finding a

^{*} djpaul@mit.edu

[†] Present address: Northrop Grumman Mission Systems, Linthicum, Maryland 21090, USA

commercial ellipsometry tool that can operate across a broad range of wavelengths, from visible to far-infrared, is challenging due to the need to adjust the optical setup of the instrument, including the source, lenses, and detectors, as the wavelength increases. FTIR spectroscopy, on the other hand, is well-suited for infrared spectroscopy and is widely available, with capabilities extending to 50 μm or beyond. FTIR-based refractive index measurements have been reported for various materials, including organic polymers, ceramics, and semiconductors, across wavelengths up to 100 μm [21–23]. While this work focuses on characterizing superconducting thin films in the 2.5 to 25 μm wavelength range for mid-infrared SNSPD applications, the methodology for extracting complex refractive indices from reflection and transmission spectra is broadly applicable to thin films at any wavelength. Hence, this FTIR-based approach can be valuable for a wide range of photonic devices and applications by reducing dependence on specialized ellipsometry tools for refractive index measurements beyond the typical wavelength range of commercially available instruments.

In this work, we developed an optimization algorithm to extract the complex refractive indices of thin-film NbN and MoSi from their FTIR transmission and reflection spectra. We validated the consistency of the extracted Drude-Lorentz parameters using spectroscopic ellipsometry and DC resistivity measurements. Finally, we discussed the applicability of the extracted room-temperature refractive indices in calculating the mid-infrared optical absorption efficiency of SNSPDs.

FTIR based Refractive Index Measurement

In this work, we deposited NbN and MoSi films on (100)-oriented CaF_2 substrates at room temperature using an AJA Orion magnetron sputtering system. CaF_2 was chosen as the substrate due to its optical transparency in the near- and mid-infrared wavelengths [24]. The infrared transparency of the substrate allowed us to

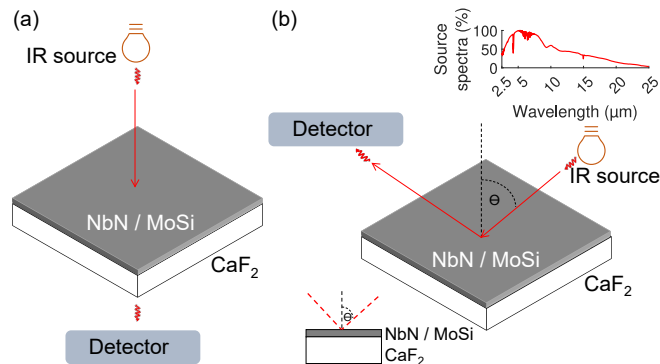


FIG. 1. A schematic representation of FTIR spectroscopy performed on the deposited NbN and MoSi films on (100)-oriented CaF_2 substrate is shown. (a) Normal incidence FTIR transmission measurement and (b) variable incidence angle FTIR reflection measurements were performed. The incidence angle, θ , was varied from 12° to 60° in the reflection measurements. FTIR source spectra are shown in the inset, with KBr used as the beam splitter and DTGS as the detector in the FTIR instrument.

measure the transmitted spectrum of the deposited thin films, which would not be possible with an opaque substrate. Undoped silicon is also a viable substrate, as it is optically transparent in the near- and mid-infrared wavelengths. We used the same optimized deposition conditions for NbN and MoSi thin films as reported in our previous works [16, 25]. The thicknesses of the deposited NbN and MoSi films on CaF_2 substrates were measured using X-ray reflectivity (XRR) and determined to be 9.93 nm and 14.981 nm, respectively. While FTIR can measure films of varying thickness, we characterized these thickness values for the NbN and MoSi films, as they fall within the typical range of superconducting film thicknesses used in SNSPD fabrication [17, 25]. The sheet resistance of the deposited NbN and MoSi films was measured to be 240.68 Ω/sq and 110.51 Ω/sq , respectively. The samples were stored in an inert atmosphere box to minimize oxidation of NbN and MoSi.

We performed FTIR reflection and transmission measurements on the samples using a Thermo Scientific Nicolet iS50. A schematic of the measurement setup is shown in Figure 1. In the reflection measurements, the reflected spectra from the sample were normalized by the reflected spectra of a gold mirror, while in the transmission measurements, source spectra were used to normalize the sample's transmitted spectra. All measurements were performed with an unpolarized collimated beam, and we conducted averaging of 64 scans per measurement with automatic atmospheric suppression enabled. To improve the accuracy of the dielectric fitting model, we measured several spectra of the sample, including transmittance at normal incidence and reflectance at incidence angles ranging from 12° to 60° . We used the Harrick specular reflection accessory for the 12° incidence angle and the Pike VeeMAX III for incidence angles from 30° to 60° .

To extract the complex refractive indices of NbN and MoSi from the measured FTIR spectra, we developed an optimization algorithm based on the transfer matrix method [21, 26]. The Drude-Lorentz oscillator model was used to describe the dielectric functions of NbN and MoSi films, as their electrical conductivity at room temperature lies between that of good metals and semiconductors [12]. The model is given by the following equation:

$$\epsilon(\omega) = \epsilon_\infty - \frac{\omega_p^2}{\omega^2 + i\omega\Gamma_D} + \sum_{k=1}^N \frac{s_k^2}{\omega_k^2 - \omega^2 - i\omega\gamma_k}$$

where ω is the spectral frequency, and ϵ_∞ is the high-frequency dielectric constant of the material. ω_p and Γ_D are the fitting parameters of the Drude model, with ω_p representing the unscreened plasma energy and Γ_D as the inverse of the free-electron relaxation time. The number of Lorentz oscillators is defined by N , where s_k , ω_k , and γ_k are the strength, resonant frequency, and damping coefficient of the k -th Lorentz oscillator, respectively. In our calculation, the frequency (ω) and the Drude-Lorentz oscillator parameters were taken in units of electron-volt.

Following the calculation of the Drude-Lorentz dielectric function, the complex refractive index of the material

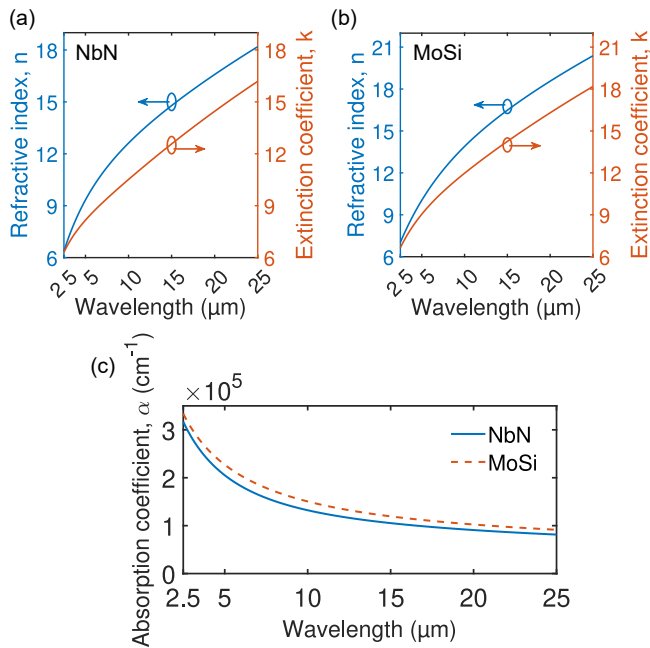


FIG. 2. Extracted mid-infrared refractive index and extinction coefficient of (a) 10-nm-thick NbN and (b) 15-nm-thick MoSi. (c) The absorption coefficient of the materials is plotted using the equation $\alpha = 4\pi k/\lambda$, where λ is the wavelength and k is the extinction coefficient.

was determined by $\overline{n(\omega)} = n(\omega) + ik(\omega) = \sqrt{\epsilon(\omega)}$ where $n(\omega)$ and $k(\omega)$ are the refractive index and extinction coefficient, respectively. Our dielectric fitting algorithm employed a nonlinear optimization function to determine the optimal values of the Drude-Lorentz oscillator parameters from an initial guess by iteratively minimizing the error between the measured FTIR spectra and the simulated spectra computed with the fitted dielectric function over the wavelength range of interest. A flowchart of the optimization routine with detailed information is provided in the supplementary Figure S1.

Mid-IR Refractive Index of NbN and MoSi

To determine the refractive indices of the deposited thin films of NbN and MoSi from the FTIR spectra, our dielectric fitting algorithm requires the dielectric function of the substrate. Although there were reported values of the refractive index of CaF₂ in the literature [24], we chose to determine it using our FTIR-based refractive index measurement method. This measurement allowed us to compare the results from our refractive index measurement method with the literature. Hence, we measured the FTIR transmission and reflection spectra of a bare CaF₂ substrate. We then applied our dielectric fitting algorithm to extract the complex refractive indices of CaF₂ from the measured FTIR spectra. The extracted refractive index values are provided in the supplementary Figure S2b, which showed good agreement with [24].

Next, we measured the FTIR spectra of 10-nm-thick NbN sample deposited on a CaF₂ substrate and determined the refractive indices of NbN between 2.5 μm and 25 μm wavelength, as shown in Figure 2(a). Similarly, we performed FTIR measurements on 15-nm-thick MoSi

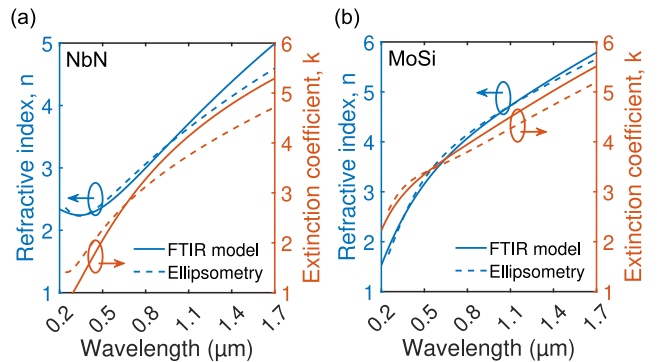


FIG. 3. Refractive indices of (a) 10-nm-thick NbN and (b) 15-nm-thick MoSi are shown in the UV to near-infrared wavelength. The solid lines represent the extrapolated values from the FTIR model, while the dotted lines represent the ellipsometry measurements.

deposited on a CaF₂ substrate and then extracted the refractive indices of MoSi, as shown in Figure 2(b). The extracted Drude-Lorentz parameters of NbN and MoSi are given in Table I.

To determine whether the extracted indices of NbN and MoSi can reproduce the experimental spectra of the thin-film samples, we simulated the transmission and reflection of the material stack, for instance, 10 nm NbN on CaF₂ and 15 nm MoSi on CaF₂, for the same incidence angle, polarization, and wavelength range used in the FTIR experiment, employing transfer matrix method. As shown in supplementary Figures S2a, S2c, and S2d, the simulated spectra using the extracted refractive indices of CaF₂, NbN, and MoSi closely matched the measured FTIR spectra. The calculated root-mean-square error (RMSE) between the simulated and FTIR-measured spectra for CaF₂, NbN, and MoSi samples were 0.969, 1.822, and 1.33, respectively, while the corresponding R-squared (R²) values were 0.999, 0.959, and 0.992, respectively. The low RMSE and high R-squared values suggest that the extracted refractive indices effectively capture the mid-infrared optical properties of these materials. In addition, we examined the wavelength-dependent mid-infrared optical absorption in these thin films by calculating their absorption coefficients, as shown in Figure 2(c). As depicted in Figure 2(c), the mid-infrared absorption coefficients of NbN and MoSi decrease with increasing wavelength, indicating that the photon absorption efficiency of NbN- and MoSi-based SNSPDs will monotonically decrease as the photon wavelength extends into the mid-infrared spectrum.

Consistency of the Fitted Drude-Lorentz Oscillators

To evaluate whether the extracted Drude-Lorentz parameters for NbN and MoSi are not overfitted to the specified mid-infrared wavelength range but are applicable across a broader spectrum, we compared the refractive indices extrapolated from these parameters in the wavelength range of 0.2 to 1.7 μm with values independently measured using the Semilab SE-2000 spectroscopic ellipsometry. Moreover, although (100)-oriented CaF₂ was used in this work as a substrate to extract the mid-infrared optical properties of NbN and MoSi, oxi-

Sample	ϵ_∞	ω_p	Γ_D	N	s_1	ω_1	γ_1	s_2	ω_2	γ_2
NbN	6.91	6.72	1.6	1	17.85	1.94	19.99			
MoSi	1.13	14.25	5.78	2	19.65	4.87	14.68	3.15	0.34	1.01

TABLE I. Extracted Drude-Lorentz oscillator parameters for 10-nm-thick NbN and 15-nm-thick MoSi films, which were obtained from the best fit of the measured FTIR data. The oscillator parameters are in units of electron-volt (eV).

dized silicon is a more conventional substrate for these thin films in SNSPD applications [16, 25]. Therefore, we chose to compare the refractive indices extrapolated from the FTIR-extracted Drude-Lorentz parameters in the range of 0.2 to 1.7 μm with the values of NbN and MoSi films of similar thickness deposited on an oxidized silicon substrate. Since the lattice constant of the (100)-oriented CaF_2 substrate is similar to that of oxidized silicon, we can consider nearly identical material growth and optical properties for NbN and MoSi on both substrates.

We deposited NbN and MoSi films on silicon substrates with 300 nm-thick thermal oxide, maintaining the same deposition conditions and adjusting the deposition time to achieve 10-nm-thick NbN and 15-nm-thick MoSi films. Subsequently, we performed spectroscopic ellipsometry measurements on the samples. The ellipsometry tool relies on reflection spectroscopy to measure changes in the polarization of reflected light at various incidence angles and wavelengths. Following the measurements, we determined the unknown refractive index of the material using an integrated analysis software by performing a best-fit optimization with various dielectric functions available in the software, such as Drude, Lorentz, Gauss, Sellmeier, and Cauchy functions. The Drude-Lorentz dielectric model was identified as the optimal model to represent the optical properties of NbN and MoSi. These measured refractive indices were then compared with the extrapolated refractive indices from our FTIR measurements, as shown in Figures 3(a) and 3(b). The extrapolated refractive indices matched reasonably well with the ellipsometric data, given that the quality and roughness of the deposited NbN and MoSi films could vary with the substrate. Nevertheless, Figures 3(a) and 3(b) show that the FTIR-extracted Drude-Lorentz parameters for NbN and MoSi performs well across the UV to mid-infrared wavelength range.

Next, we calculated the plasma wavelength and DC sheet resistance of the NbN and MoSi films using the FTIR-extracted Drude parameters to assess whether the Drude parameters are physically meaningful rather than merely fitting parameters. The plasma wavelengths of the NbN and MoSi films can be estimated from their Drude parameter ω_p using $\lambda_p[\text{nm}] = 1239.8/\omega_p[\text{eV}]$. We calculated the plasma wavelength to be 87.03 nm for 15-nm-thick MoSi and 184.6 nm for 10-nm-thick NbN. In the literature [12], the plasma wavelength of 11.7-nm-thick NbN is reported as 139.1 nm, which is consistent with our calculated value.

In addition, the DC resistivity of the films can be calculated using $\rho_n = (\Gamma_D \hbar)/(\omega_p^2 \epsilon_0 e)$. Here, ϵ_0 is the free-space permittivity, e is the electron charge, and \hbar

is the reduced Planck constant. The Drude parameter values, ω_p and Γ_D , for NbN and MoSi, were taken from Table I. We calculated the DC resistivity (ρ_n) of the 10-nm-thick NbN and 15-nm-thick MoSi films and subsequently determined their corresponding sheet resistances using $R_{sheet} = \rho_n/\text{thickness}$. This resulted in sheet resistances of 264.04 Ω/sq and 141.38 Ω/sq for NbN and MoSi films, respectively, which are close to the measured room-temperature values of 240.68 Ω/sq and 110.51 Ω/sq . Hence, we infer that the extracted Drude-Lorentz parameters for thin-film NbN and MoSi demonstrate physical consistency and effectively describe their optical behavior across the UV to mid-infrared range.

Refractive Indices of NbN and MoSi below T_c

In this work, we determined the mid-infrared refractive indices of NbN and MoSi using room-temperature FTIR spectroscopy; however, our primary interest lies in the optical properties of these materials in their superconducting state for performing optical simulations of SNSPDs and other superconducting photonic devices. The prevailing view in the literature is that the optical constants of a superconductor below T_c should not deviate substantially from its room-temperature values when the photon energy is well above the superconducting gap energy [12, 13]. The superconducting gap energy of thin-film NbN and MoSi can be estimated from their critical temperatures using the relation $3.52 \times k_B T_c$ [27], where k_B is the Boltzmann constant and T_c is the critical temperature of the superconducting thin film. The critical temperatures of the deposited NbN and MoSi thin films were around 6 K, corresponding to the superconducting gap energy of approximately 2 meV. This energy corresponds to photon wavelength of 600 μm , which is much longer than the wavelengths considered in this work. Therefore, the refractive indices extracted in the wavelength range of 2.5 to 25 μm using FTIR measurements should closely approximate the refractive index at temperatures below T_c and hence be suitable for use in the design of superconducting photonic devices. Further discussion is provided in the supplementary information.

Conclusion

In summary, we determined the mid-infrared refractive indices of 10-nm-thick NbN and 15-nm-thick MoSi using room-temperature FTIR spectroscopy. The accuracy of the extracted optical properties was validated with spectroscopic ellipsometry and DC sheet resistance measurements. While further optimization of the stoichiometry and thickness of the NbN and MoSi films will be required to enhance the mid-infrared photon detection sensitivity of SNSPDs, the results presented here will be useful for

characterizing and understanding the optical properties of these films. Furthermore, this approach for determining refractive indices using FTIR spectroscopy will be effective for extracting the optical properties of thin films of various materials in the mid- to far-infrared wavelengths, where obtaining a specialized ellipsometry tool for that wavelength range may be challenging.

ACKNOWLEDGMENTS

This work was carried out in part through the use of MIT.nano’s facilities, and the authors would like to thank Tim McClure of the MIT Materials Research Laboratory (MRL) for the technical support related to FTIR. The authors also thank Francesca Incalza, Matthew Yeung,

and Phillip D. Keathley for their feedback during the preparation of the manuscript. The initial stage of this research was sponsored by the US Army Research Office (ARO) and was accomplished under Cooperative Agreement No. W911NF-21-2-0041. The later stages of this research were supported by MIT Lincoln Laboratory under the SNSPD-SFQ Line program and by the National Science Foundation under Grant No. EEC-1941583.

Code Availability

Source codes used to extract the refractive indices of NbN and MoSi from FTIR measurements are available on GitHub (<https://github.com/DipJotiPaul/RefractEx>).

-
- [1] J. Haas and B. Mizaikoff, Advances in mid-infrared spectroscopy for chemical analysis, *Annual Review of Analytical Chemistry* **9**, 45 (2016).
- [2] J. A. Lau, V. B. Verma, D. Schwarzer, and A. M. Wodtke, Superconducting single-photon detectors in the mid-infrared for physical chemistry and spectroscopy, *Chemical Society Reviews* **52**, 921 (2023).
- [3] V. Verma, B. Korzh, A. B. Walter, A. E. Lita, R. M. Briggs, M. Colangelo, Y. Zhai, E. E. Wollman, A. D. Beyer, J. P. Allmaras, *et al.*, Single-photon detection in the mid-infrared up to 10 μm wavelength using tungsten silicide superconducting nanowire detectors, *APL Photonics* **6** (2021).
- [4] G. G. Taylor, A. B. Walter, B. Korzh, B. Bumble, S. R. Patel, J. P. Allmaras, A. D. Beyer, R. O’Brien, M. D. Shaw, and E. E. Wollman, Low-noise single-photon counting superconducting nanowire detectors at infrared wavelengths up to 29 μm , *Optica* **10**, 1672 (2023).
- [5] V. Verma, B. Korzh, E. Wollman, Y. Zhai, A. Walter, E. Schmidt, A. Lita, J. Allmaras, M. Shaw, R. Mirin, *et al.*, Superconducting nanowire single photon detectors and detector arrays in the mid-infrared, in *Advanced Photon Counting Techniques XVI*, Vol. 12089 (SPIE, 2022) pp. 50–55.
- [6] E. E. Wollman, G. Taylor, S. Patel, B. Bumble, B. Korzh, M. Colangelo, D. J. Paul, S. van Berkel, A. Walter, J. Allmaras, *et al.*, Current state of mid-infrared superconducting nanowire single-photon detectors, in *X-Ray, Optical, and Infrared Detectors for Astronomy XI* (SPIE, 2024) p. PC1310306.
- [7] J. Chiles, I. Charaev, R. Lasenby, M. Baryakhtar, J. Huang, A. Roshko, G. Burton, M. Colangelo, K. Van Tilburg, A. Arvanitaki, *et al.*, New constraints on dark photon dark matter with superconducting nanowire detectors in an optical haloscope, *Physical Review Letters* **128**, 231802 (2022).
- [8] E. E. Wollman, V. B. Verma, A. B. Walter, J. Chiles, B. Korzh, J. P. Allmaras, Y. Zhai, A. E. Lita, A. N. McCaughan, E. Schmidt, *et al.*, Recent advances in superconducting nanowire single-photon detector technology for exoplanet transit spectroscopy in the mid-infrared, *Journal of Astronomical Telescopes, Instruments, and Systems* **7**, 011004 (2021).
- [9] J. Liu, K. Dona, G. Hoshino, S. Knirck, N. Kurinsky, M. Malaker, D. W. Miller, A. Sonnenschein, M. H. Awida, P. S. Barry, *et al.*, Broadband solenoidal haloscope for terahertz axion detection, *Physical Review Letters* **128**, 131801 (2022).
- [10] G. G. Taylor, D. Morozov, N. R. Gemmell, K. Erotokritou, S. Miki, H. Terai, and R. H. Hadfield, Photon counting LIDAR at 2.3 μm wavelength with superconducting nanowires, *Optics Express* **27**, 38147 (2019).
- [11] F. Wang, F. Ren, Z. Ma, L. Qu, R. Gourgues, C. Xu, A. Baghdasaryan, J. Li, I. E. Zadeh, J. W. Los, *et al.*, In vivo non-invasive confocal fluorescence imaging beyond 1,700 nm using superconducting nanowire single-photon detectors, *Nature Nanotechnology* **17**, 653 (2022).
- [12] A. Semenov, B. Günther, U. Böttger, H.-W. Hübers, H. Bartolf, A. Engel, A. Schilling, K. Ilin, M. Siegel, R. Schneider, *et al.*, Optical and transport properties of ultrathin NbN films and nanostructures, *Physical Review B* **80**, 054510 (2009).
- [13] A. Banerjee, R. M. Heath, D. Morozov, D. Hemakumara, U. Nasti, I. Thayne, and R. H. Hadfield, Optical properties of refractory metal based thin films, *Optical Materials Express* **8**, 2072 (2018).
- [14] R. M. Heath, M. G. Tanner, T. D. Drysdale, S. Miki, V. Giannini, S. A. Maier, and R. H. Hadfield, Nanoantenna enhancement for telecom-wavelength superconducting single photon detectors, *Nano Letters* **15**, 819 (2015).
- [15] R. Blanchard, S. V. Boriskina, P. Genevet, M. A. Kats, J.-P. Tetienne, N. Yu, M. O. Scully, L. Dal Negro, and F. Capasso, Multi-wavelength mid-infrared plasmonic antennas with single nanoscale focal point, *Optics Express* **19**, 22113 (2011).
- [16] A. E. Dane, A. N. McCaughan, D. Zhu, Q. Zhao, C.-S. Kim, N. Calandri, A. Agarwal, F. Bellei, and K. K. Berggren, Bias sputtered NbN and superconducting nanowire devices, *Applied Physics Letters* **111** (2017).
- [17] F. Marsili, F. Bellei, F. Najafi, A. E. Dane, E. A. Dauler, R. J. Molnar, and K. K. Berggren, Efficient single photon detection from 500 nm to 5 μm wavelength, *Nano Letters* **12**, 4799 (2012).
- [18] Y. Pan, H. Zhou, L. Zhang, H. Li, Y. Tang, H. Yu, M. Si, L. You, and Z. Wang, Superconducting nanowire single-

- photon detector made of ultrathin γ -Nb₄N₃ film for mid-infrared wavelengths, *Superconductor Science and Technology* **34**, 074001 (2021).
- [19] Q. Chen, R. Ge, L. Zhang, F. Li, B. Zhang, Y. Dai, Y. Fei, X. Wang, X. Jia, Q. Zhao, *et al.*, Mid-infrared single photon detector with superconductor Mo_{0.8}Si_{0.2} nanowire, arXiv preprint arXiv:2011.06699 (2020).
- [20] P. Karl, M. Ubl, M. Hentschel, P. Flad, Z.-Y. Chiao, J.-W. Yang, Y.-J. Lu, and H. Giessen, Optical properties of niobium nitride plasmonic nanoantennas for the near- and mid-infrared spectral range, *Optical Materials Express* **10**, 2597 (2020).
- [21] A. Srinivasan, B. Czaplá, J. Mayo, and A. Narayanaswamy, Infrared dielectric function of polydimethylsiloxane and selective emission behavior, *Applied Physics Letters* **109** (2016).
- [22] C. Metaxa, B. D. Ozsdolay, T. Zorba, K. Paraskevopoulos, D. Gall, and P. Patsalas, Electronic and optical properties of rocksalt-phase tungsten nitride (B1-WN), *Journal of Vacuum Science & Technology A* **35** (2017).
- [23] L. W. Perner, G.-W. Truong, D. Follman, M. Prinz, G. Winkler, S. Puchegger, G. D. Cole, and O. H. Heckl, Simultaneous measurement of mid-infrared refractive indices in thin-film heterostructures: methodology and results for GaAs/AlGaAs, *Physical Review Research* **5**, 033048 (2023).
- [24] W. Kaiser, W. Spitzer, R. Kaiser, and L. Howarth, Infrared properties of CaF₂, SrF₂, and BaF₂, *Physical Review* **127**, 1950 (1962).
- [25] I. Charaev, Y. Morimoto, A. Dane, A. Agarwal, M. Colangelo, and K. K. Berggren, Large-area microwire MoSi single-photon detectors at 1550 nm wavelength, *Applied Physics Letters* **116** (2020).
- [26] M. C. Tropicovsky, A. S. Sabau, A. R. Lupini, and Z. Zhang, Transfer-matrix formalism for the calculation of optical response in multilayer systems: from coherent to incoherent interference, *Optics Express* **18**, 24715 (2010).
- [27] J. Bardeen, L. N. Cooper, and J. R. Schrieffer, Theory of superconductivity, *Physical Review* **108**, 1175 (1957).

Supplementary Information

**Determination of Mid-Infrared Refractive Indices of
Superconducting Thin Films Using Fourier Transform Infrared
Spectroscopy**

Dip Joti Paul, Tony X. Zhou, and Karl K. Berggren

*Research Laboratory of Electronics, Massachusetts
Institute of Technology, Cambridge, MA 02139, USA*

arXiv:2503.00169v1 [physics.optics] 28 Feb 2025

METHODS

A. Refractive Index Extraction from FTIR Spectra

To extract the refractive indices of NbN and MoSi from the measured FTIR spectra, we developed a dielectric constant fitting program based on the transfer-matrix method. The program can simulate the transmission and reflection spectra of a sample at specified incidence angles, polarization angles, and wavelengths, given that the thickness and refractive indices of the constituent materials of the sample are known at those wavelengths. To extract the refractive index of a material from its FTIR spectra, we added an optimization routine to the program, as shown in Figure S1. The input data for the program include the FTIR transmission and reflection spectra of the sample, the incidence angle values of the corresponding spectra, and the thickness of the different material layers in the sample. All our FTIR measurements were performed with an unpolarized beam. Additionally, the refractive indices of the known materials in the sample stack were fed into the program, and we assumed a suitable dielectric constant model for the unknown material. In this work, we employed the Drude-Lorentz dielectric model to describe the optical properties of NbN and MoSi. Since the Drude-Lorentz dielectric model inherently ensures Kramers–Kronig (KK) consistency between the real and imaginary parts of the optical constants [1, 2], a separate

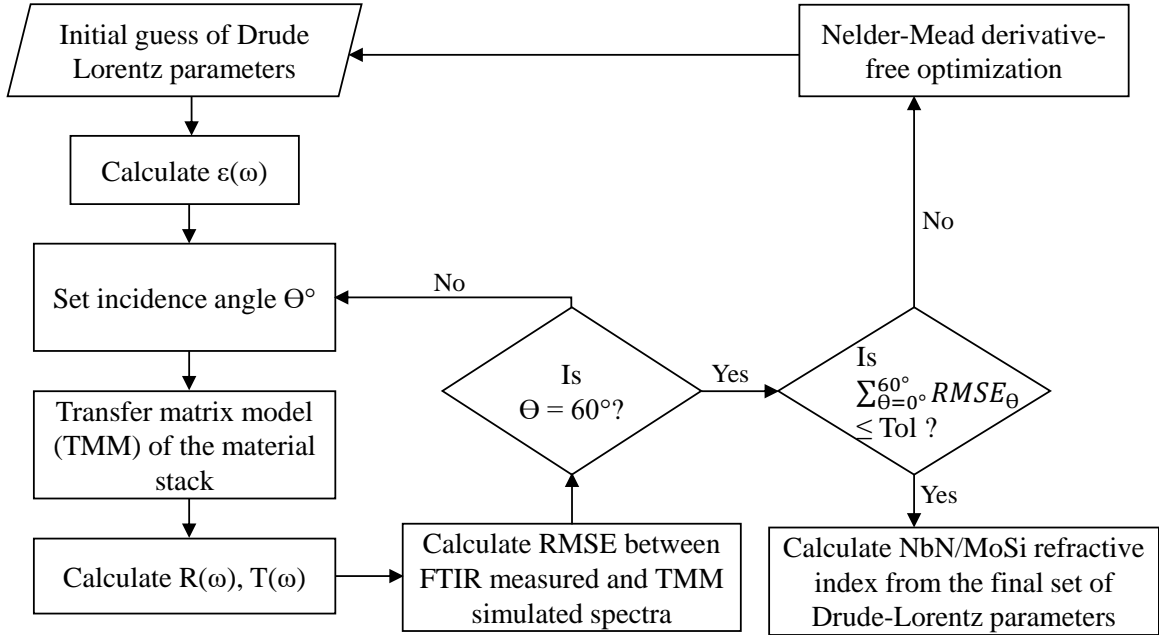


FIG. S1. A flowchart of the dielectric fitting optimization algorithm is shown, which was used to extract the refractive indices of the unknown material from the measured FTIR transmission and reflection spectra.

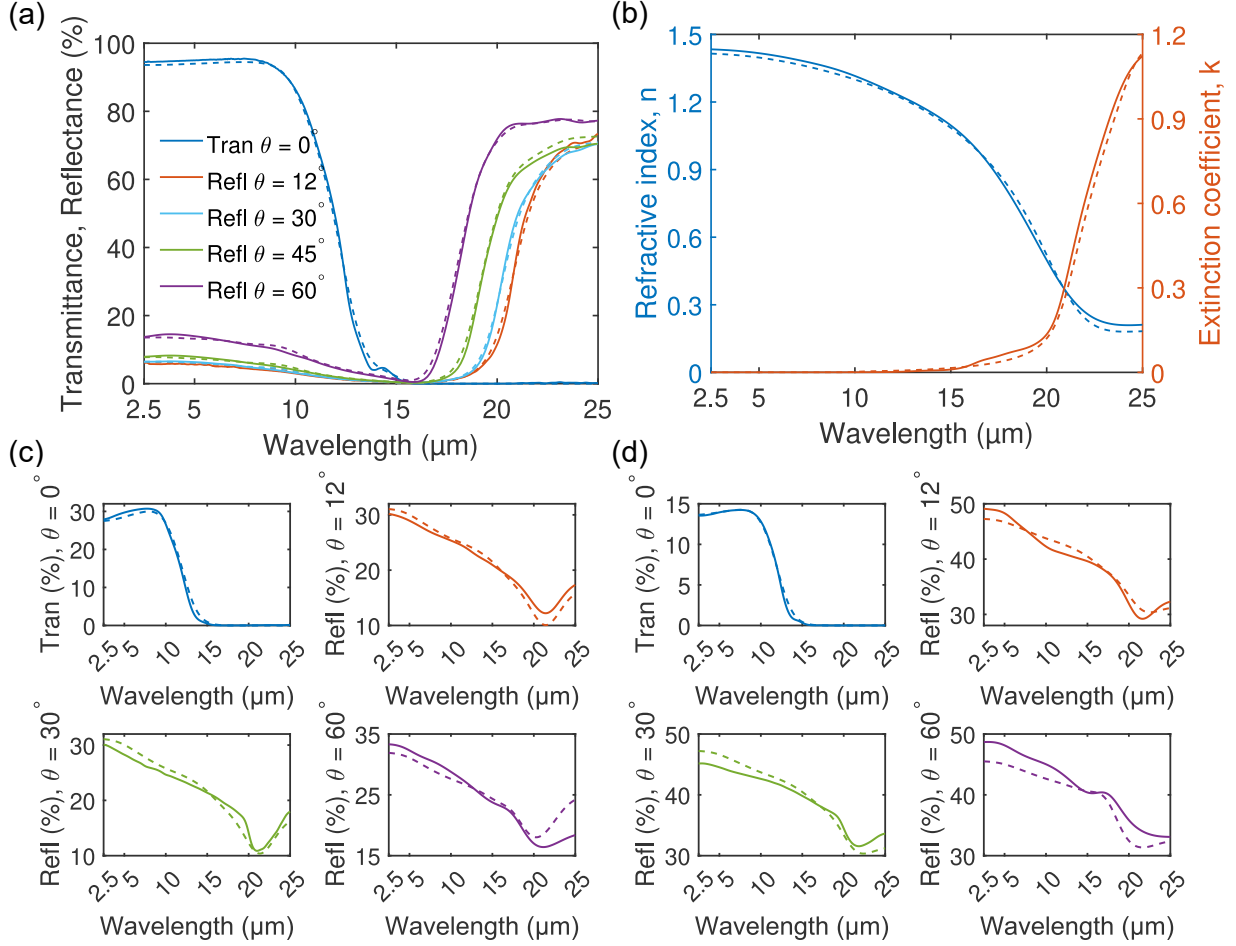


FIG. S2. (a) Transmittance and reflectance spectra of bare CaF_2 obtained from FTIR measurements (solid line) and the dielectric fitting simulation using the extracted refractive indices of CaF_2 (dashed line). (b) Refractive indices of CaF_2 from our dielectric fitting simulation (solid line) and the literature [3] (dashed line). (c) FTIR transmittance and reflectance spectra (solid line) of 10-nm-thick NbN on CaF_2 and corresponding simulated spectra using the extracted refractive indices of NbN and CaF_2 (dashed line). (d) FTIR spectra (solid line) and corresponding simulated spectra (dashed line) of 15-nm-thick MoSi on CaF_2 .

KK analysis was not performed in the dielectric fitting optimization algorithm.

The dielectric fitting algorithm employs a nonlinear optimization function, namely the Nelder-Mead algorithm, to find the final set of Drude-Lorentz parameters from the initial guess by minimizing a root-mean-square error (RMSE) function over the wavelength range of interest. The root-mean-square error function is given by

$$\sqrt{\frac{1}{M \times N} \sum_{j=1}^M \sum_{\lambda=2.5\mu\text{m}}^{25\mu\text{m}} [X_{(meas,j)}(\lambda) - X_{(calc,j)}(\lambda)]^2}$$

where M is the total number of FTIR spectra measured for the sample, N is the total num-

ber of wavelength points in the FTIR spectra, $X_{(meas,j)}(\lambda)$ and $X_{(calc,j)}(\lambda)$ are the transmittance/reflectance spectra obtained from FTIR measurement and calculation, respectively.

The optimization program iteratively updates the unknown parameters until the error function value drops below the given tolerance value. We used one transmission spectrum and several reflection spectra of the sample measured at various incidence angles to perform the dielectric fitting optimization, as shown in Figure S2. First, we measured the FTIR transmission and reflection spectra of bare CaF₂ and extracted its refractive indices, as shown in Figure S2(b). Then, the extracted refractive indices of CaF₂ were fed into the dielectric extraction optimization routine for NbN and MoSi to calculate their refractive indices from their measured FTIR spectra.

B. Calculation of DC Resistivity from Drude Dielectric Coefficients

The dielectric functions of metals, conductive oxides, and heavily doped semiconductors are typically modeled using the Drude-Lorentz model. The Drude term accounts for the intraband transition of free electrons in the material, and it is characterized by two parameters: the plasma frequency (ω_p) and a broadening factor related to the free electron lifetime (Γ_D). Following the equations in [4, 5], the density of conduction electrons in a material can be calculated from its unscreened plasma energy (ω_p) using $N = (\omega_p^2 \epsilon_0 m^*) / (e^2 \hbar^2)$. Here ϵ_0 is the free-space permittivity, m^* is the electron effective mass, e is the electron charge, and \hbar is the reduced Planck constant. The other Drude parameter, Γ_D , is associated with the scattering of conduction electrons in the material. According to the free-electron model, the relaxation time of the conduction electrons is given by $\tau = \hbar / \Gamma_D$ [5]. In addition, the relaxation time is related to the room-temperature resistivity (ρ_n) of the film by the equation $\rho_n = m^* / (\tau N e^2)$ [4, 5]. By substituting the values of τ and N in this equation, we get

$$\rho_n = \frac{\Gamma_D \hbar}{\omega_p^2 \epsilon_0 e}$$

Thus, by obtaining the fitted Drude parameters, namely ω_p and Γ_D , for NbN and MoSi from our refractive index extraction algorithm, we can calculate the room-temperature resistivity values of the films.

C. Refractive Indices of Superconductors Below T_c

In this section, we discuss the validity of using the room-temperature mid-infrared refractive indices of NbN and MoSi to represent their refractive indices at cryogenic temperatures.

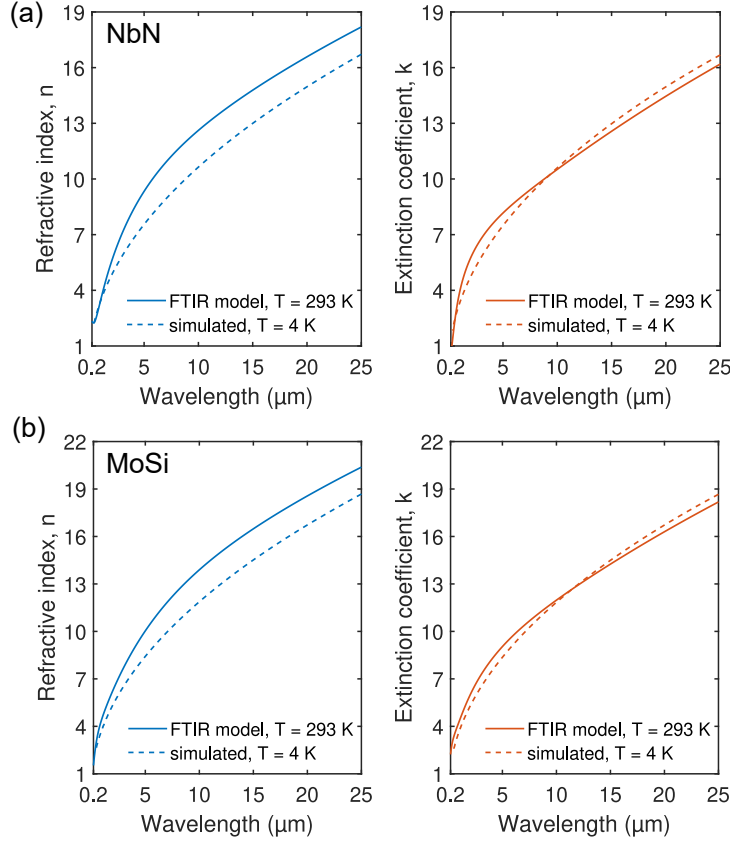


FIG. S3. The refractive index and extinction coefficient of (a) 10-nm-thick NbN and (b) 15-nm-thick MoSi films are shown, which were extracted using room-temperature FTIR measurements (solid lines) and simulated using the Mattis–Bardeen model for $T = 4\text{ K}$ (dashed lines). In the simulation model, the critical temperatures (T_c) of the 10-nm-thick NbN and 15-nm-thick MoSi were taken as 6.7 K and 5.4 K, respectively.

At zero temperature, an ideal superconductor does not absorb optical radiation with energies lower than its superconducting gap energy ($2\Delta_0$). However, when the photon energy is well above the superconducting gap energy, an individual quantum of electromagnetic radiation can break a Cooper pair and generate two excited quasiparticles. This leads to dissipation in the superconductor, and the optical conductivity of the superconducting film below its critical temperature (T_c) can be derived using the Mattis–Bardeen model [6, 7]:

$$\begin{aligned} \epsilon'_{rs}|_{\hbar\omega < 2\Delta} &= 1 - \frac{\sigma_n}{\hbar\epsilon_0\omega^2} \int_{\Delta-\hbar\omega}^{\Delta} [1 - 2f(E + \hbar\omega)] \times \frac{[E^2 + \Delta^2 + \hbar\omega E]}{[\Delta^2 - E^2]^{1/2}[(E + \hbar\omega)^2 - \Delta^2]^{1/2}} dE \\ \epsilon'_{rs}|_{\hbar\omega > 2\Delta} &= 1 - \frac{\sigma_n}{\hbar\epsilon_0\omega^2} \int_{-\Delta}^{\Delta} [1 - 2f(E + \hbar\omega)] \times \frac{[E^2 + \Delta^2 + \hbar\omega E]}{[\Delta^2 - E^2]^{1/2}[(E + \hbar\omega)^2 - \Delta^2]^{1/2}} dE \end{aligned} \quad (1)$$

$$\epsilon''_{rs} = \frac{2\sigma_n}{\hbar\epsilon_0\omega^2} \int_{\Delta}^{\infty} [f(E) - f(E + \hbar\omega)]g(E) dE + \int_{\Delta-\hbar\omega}^{-\Delta} [1 - 2f(E + \hbar\omega)]g(E) dE \quad (2)$$

here σ_n is the normal state conductivity, $f(E) = 1/(1 + \exp(E/k_B T))$ is the Fermi-Dirac function, and $g(E) = [E^2 + \Delta^2 + \hbar\omega E]/([E^2 - \Delta^2]^{1/2}[(E + \hbar\omega)^2 - \Delta^2]^{1/2})$ is the density of state. The term 2Δ represents the superconducting gap energy at $T = 0$ K. For temperatures $T < T_c$, we can find $\Delta = 1.74 \times \Delta_{T=0} \sqrt{1 - (T/T_c)}$. The value of σ_n can be calculated from the inverse of the room-temperature resistivity (ρ_n) of the film.

Finally, the complex refractive index of the superconducting film is given by $n + ik = \sqrt{\epsilon'_{rs} + i\epsilon''_{rs}}$ where n and k are the refractive index and extinction coefficient, respectively. The Mattis–Bardeen model has been applied to different type-I and type-II BCS superconducting thin films previously and has shown good agreement with experimental results [8–10]. Figure S3 shows the calculated refractive indices of NbN and MoSi below their critical temperatures using the Mattis–Bardeen model, compared with the values measured at room temperature via FTIR spectroscopy. The plot suggests that the optical properties of the superconductors at room temperature provide a good approximation of their properties at cryogenic temperatures. This aligns with the commonly held perception in the literature [11, 12], as SNSPDs are often designed using the room-temperature refractive indices of superconducting materials [11–13]. Our calculation shows that this assumption holds true for the mid-infrared spectrum.

-
- [1] T. C. Asmara, I. Santoso, and A. Rusydi, Self-consistent iteration procedure in analyzing reflectivity and spectroscopic ellipsometry data of multilayered materials and their interfaces, *Review of Scientific Instruments* **85** (2014).
 - [2] A. Kuzmenko, Kramers–Kronig constrained variational analysis of optical spectra, *Review of Scientific Instruments* **76** (2005).
 - [3] W. Kaiser, W. Spitzer, R. Kaiser, and L. Howarth, Infrared properties of CaF₂, SrF₂, and BaF₂, *Physical Review* **127**, 1950 (1962).
 - [4] P. Patsalas and S. Logothetidis, Optical, electronic, and transport properties of nanocrystalline titanium nitride thin films, *Journal of Applied Physics* **90**, 4725 (2001).
 - [5] C. Metaxa, B. D. Ozsdolay, T. Zorba, K. Paraskevopoulos, D. Gall, and P. Patsalas, Electronic and optical properties of rocksalt-phase tungsten nitride (B1-WN), *Journal of Vacuum Science & Technology A* **35** (2017).

- [6] D. C. Mattis and J. Bardeen, Theory of the anomalous skin effect in normal and superconducting metals, *Physical Review* **111**, 412 (1958).
- [7] A. H. Majedi, Theoretical investigations on THz and optical superconductive surface plasmon interface, *IEEE Transactions on Applied Superconductivity* **19**, 907 (2009).
- [8] R. Glover III and M. Tinkham, Conductivity of superconducting films for photon energies between 0.3 and 40 kT_c, *Physical Review* **108**, 243 (1957).
- [9] X. Xi, J.-H. Park, D. Graf, G. Carr, and D. Tanner, Infrared vortex-state electrodynamics in type-II superconducting thin films, *Physical Review B—Condensed Matter and Materials Physics* **87**, 184503 (2013).
- [10] R. Cervasio, L. Tomarchio, M. Verseils, J.-B. Brubach, S. Macis, S. Zeng, A. Ariando, P. Roy, and S. Lupi, Optical properties of superconducting Nd_{0.8}Sr_{0.2}NiO₂ nickelate, *ACS Applied Electronic Materials* **5**, 4770 (2023).
- [11] A. Banerjee, R. M. Heath, D. Morozov, D. Hemakumara, U. Nasti, I. Thayne, and R. H. Hadfield, Optical properties of refractory metal based thin films, *Optical Materials Express* **8**, 2072 (2018).
- [12] A. Semenov, B. Günther, U. Böttger, H.-W. Hübbers, H. Bartolf, A. Engel, A. Schilling, K. Ilin, M. Siegel, R. Schneider, *et al.*, Optical and transport properties of ultrathin NbN films and nanostructures, *Physical Review B* **80**, 054510 (2009).
- [13] V. Verma, B. Korzh, A. B. Walter, A. E. Lita, R. M. Briggs, M. Colangelo, Y. Zhai, E. E. Wollman, A. D. Beyer, J. P. Allmaras, *et al.*, Single-photon detection in the mid-infrared up to 10 μm wavelength using tungsten silicide superconducting nanowire detectors, *APL Photonics* **6** (2021).